

# PROCEEDINGS OF SPIE

## ***Optical Design and Engineering IV***

**Laurent Mazuray**  
**Rolf Wartmann**  
**Andrew Wood**  
**Jean-Luc M. Tissot**  
**Jeffrey M. Raynor**  
*Editors*

**5–8 September 2011**  
**Marseille, France**

*Sponsored by*  
SPIE

*Coorganised by*  
POPsud - Optitec (France)

*Cosponsored by*  
Communauté Urbaine Marseille Provence Métropole (France)  
Ville de Marseille (France)

*Cooperating Organisation*  
Schott AG (Germany)

*Published by*  
SPIE

**Volume 8167**

Proceedings of SPIE, 0277-786X, v. 8167

SPIE is an international society advancing an interdisciplinary approach to the science and application of light.

The papers included in this volume were part of the technical conference cited on the cover and title page. Papers were selected and subject to review by the editors and conference program committee. Some conference presentations may not be available for publication. The papers published in these proceedings reflect the work and thoughts of the authors and are published herein as submitted. The publisher is not responsible for the validity of the information or for any outcomes resulting from reliance thereon.

Please use the following format to cite material from this book:

Author(s), "Title of Paper," in *Optical Design and Engineering IV*, edited by Laurent Mazuray, Rolf Wartmann, Andrew Wood, Jean-Luc M. Tissot, Jeffrey M. Raynor, Proceedings of SPIE Vol. 8167 (SPIE, Bellingham, WA, 2011) Article CID Number.

ISSN 0277-786X  
ISBN 9780819487933

Published by

**SPIE**

P.O. Box 10, Bellingham, Washington 98227-0010 USA  
Telephone +1 360 676 3290 (Pacific Time) · Fax +1 360 647 1445  
SPIE.org

Copyright © 2011, Society of Photo-Optical Instrumentation Engineers

Copying of material in this book for internal or personal use, or for the internal or personal use of specific clients, beyond the fair use provisions granted by the U.S. Copyright Law is authorized by SPIE subject to payment of copying fees. The Transactional Reporting Service base fee for this volume is \$18.00 per article (or portion thereof), which should be paid directly to the Copyright Clearance Center (CCC), 222 Rosewood Drive, Danvers, MA 01923. Payment may also be made electronically through CCC Online at [copyright.com](http://copyright.com). Other copying for republication, resale, advertising or promotion, or any form of systematic or multiple reproduction of any material in this book is prohibited except with permission in writing from the publisher. The CCC fee code is 0277-786X/11/\$18.00.

Printed in the United States of America.

Publication of record for individual papers is online in the SPIE Digital Library.

The logo for SPIE Digital Library features the word "SPIE" in a bold, sans-serif font above the words "Digital Library" in a smaller, similar font. To the right of the text is a stylized graphic consisting of three vertical bars of increasing height, resembling a bar chart or a signal waveform.

[SPIDigitalLibrary.org](http://SPIDigitalLibrary.org)

---

**Paper Numbering:** Proceedings of SPIE follow an e-First publication model, with papers published first online and then in print and on CD-ROM. Papers are published as they are submitted and meet publication criteria. A unique, consistent, permanent citation identifier (CID) number is assigned to each article at the time of the first publication. Utilization of CIDs allows articles to be fully citable as soon as they are published online, and connects the same identifier to all online, print, and electronic versions of the publication. SPIE uses a six-digit CID article numbering system in which:

- The first four digits correspond to the SPIE volume number.
- The last two digits indicate publication order within the volume using a Base 36 numbering system employing both numerals and letters. These two-number sets start with 00, 01, 02, 03, 04, 05, 06, 07, 08, 09, 0A, 0B ... 0Z, followed by 10-1Z, 20-2Z, etc.

The CID number appears on each page of the manuscript. The complete citation is used on the first page, and an abbreviated version on subsequent pages. Numbers in the index correspond to the last two digits of the six-digit CID number.

# Contents

xiii Conference Committee

## **PART A Optical Design and Engineering IV**

---

### **DESIGN THEORY AND TECHNIQUES I**

---

- 8167 02 **Optical glass: dispersion in the near infrared (Invited Paper)** [8167A-01]  
P. Hartmann, SCHOTT AG (Germany)
- 8167 03 **Method to allocate freeform surfaces in axially asymmetric optical systems** [8167A-02]  
A. Yabe, Consultant (Germany)
- 8167 04 **Original design rules for simple imaging systems** [8167A-03]  
F. de la Barrière, G. Druart, N. Guérineau, ONERA (France); J. Taboury, Institut d'Optique (France)
- 8167 05 **An opto-mechanical model and stray light investigation of laser treated human eye** [8167A-04]  
K. Frey, M. Palme, T. Peschel, S. Riehemann, G. Notni, Fraunhofer-Institut für Angewandte Optik und Feinmechanik (Germany)

---

### **DESIGN THEORY AND TECHNIQUES II**

---

- 8167 06 **Considering the pupil coordinate of aberration theory from the view point of the sine condition in the presence of spherical aberration** [8167A-05]  
M. Shibuya, Tokyo Polytechnic Univ. (Japan) and Topcon Corp. (Japan)
- 8167 07 **Freeform lens for an efficient wall washer** [8167A-06]  
A. Bruneton, RWTH Aachen Univ. (Germany); A. Bäuerle, P. Loosen, RWTH Aachen Univ. (Germany) and Fraunhofer-Institut für Lasertechnik (Germany); R. Wester, Fraunhofer-Institut für Lasertechnik (Germany)
- 8167 08 **Design and simulation of diffractive optical components in fast optical imaging systems** [8167A-07]  
A. M. Herkommer, R. Reichle, M. Häfner, C. Pruss, Univ. Stuttgart (Germany)
- 8167 09 **Analysis of the diffraction efficiency of reflection and transmission holographic gratings by means of a parallel FDTD approach** [8167A-08]  
J. Francés, S. Bleda, S. Gallego, C. Neipp, A. Márquez, I. Pascual, A. Beléndez, Univ. de Alicante (Spain)

# Analysis of the diffraction efficiency of reflection and transmission holographic gratings by means of a parallel FDTD approach

J. Francés\*<sup>a</sup>, S. Bleda<sup>a,b</sup>, S. Gallego<sup>a,b</sup>, C. Neipp<sup>a,b</sup>, A. Márquez<sup>a,b</sup>, I. Pascual<sup>b,c</sup>, A. Beléndez<sup>a,b</sup>

<sup>a</sup>Dpto. de Física, Ingeniería de Sistemas y Teoría de la Señal, Universidad de Alicante/Ctra. San Vicente del Raspeig, San Vicente del Raspeig, Alicante, España E-03080

<sup>b</sup>Instituto Universitario de Física Aplicada a las Ciencias y las Tecnologías, Universidad de Alicante /Ctra. San Vicente del Raspeig, San Vicente del Raspeig, Alicante, España E-03080

<sup>c</sup>Dpto. De Óptica, Farmacología y Anatomía, Universidad de Alicante/Ctra. San Vicente del Raspeig, San Vicente del Raspeig, Alicante, España E-03080

## ABSTRACT

In this work a vectorized and parallel version of the Finite-Difference Time-Domain method (FDTD) is applied to Volume Holographic Gratings (VHG) and Thin-Film Filters (TFF). In particular, in this work gratings with a grating period vector forming an arbitrary angle with the perpendicular to the plane of incidence are analyzed. Angular and wavelength selectivity are obtained by means of the normalized diffraction efficiency. These parameters are positively compared with experimental values and also with analytical closed expressions, thus validating our method. Furthermore, analysis of the performance of the parallel method is shown obtaining a severe improvement with respect to the classical version of the FDTD method. This improvement of the algorithm provides a feasible and accurate scheme for simulating a wide range of optical devices.

**Keywords:** FDTD, holography, diffraction grating, diffraction efficiency, parallelism, SpeedUp, vectorization

## 1. INTRODUCTION

The importance of designing and manufacturing of diffractive optical elements has produced a growth of researches in this field since the nineteenth century. For instance, the most significant development, from the thin-film point of view, was the Fabry-Perot interferometer<sup>1</sup> described in 1899, which has become one of the basic structures for Thin-Film Filters<sup>2</sup> (TFF). The most significant application related with the holography can be found later and almost simultaneously by several groups, and it was related with holographic interferometry<sup>3-5</sup>.

The developments in diffractive optics in the last years have been the basis of a wide spectrum of devices used in many applications such as broadband communications<sup>6</sup> or data storage<sup>7</sup>.

Therefore, it is necessary a robust and efficient method for simulating and obtaining specific information related with the electromagnetic field. For that matter, a great number of numerical methods have been developed in order to solve the Maxwell's curl equations. These methods can be easily classified into three families: Finite Element Methods (FEM), Boundary Element Method (BEM) and Finite Difference methods (FD). Regarding the first two methods, it must be said that have been widely used for modal analysis in electromagnetics and other fields. Concerning FD, it has been used for transient analysis (FD Time-Domain) and in many areas such as electromagnetism, acoustics and vibrations. Due to the fact that the time costs of the FD method were unaffordable for several applications, it was relegated to specific applications. Nevertheless, with actual multi-core processors available in the market the time costs for this method have been reduced dramatically.

In this work a vectorial and parallel version of the FDTD in two dimensions has been implemented in order to take advantage of the multi-cores available in modern Central Processor Units (CPU), and also a vectorization of the instructions related with the method has been done for using the Streaming SIMD Extensions (SSE). Therefore, using these extensions four basic arithmetic operations can be evaluated in a single CPU clock cycle<sup>8</sup>.

The improved FDTD method has been applied to several optical devices such as VHG and TFF. Regarding VHGs, volume reflection gratings have been analyzed by the FDTD method and the reflectance has been obtained as a function

of the angle of incidence of the grating. The volume holograms are a system of layers corresponding to a periodic variation of refractive index, and the diffracted amplitude reaches its higher value only when the Bragg condition is satisfied<sup>11</sup>. The refractive index  $n$  is assumed to vary sinusoidally by the relation

$$n = n_0 + n_1 \cos[K(\cos \varphi y + \sin \varphi x)] \tag{1}$$

where in this case  $n_0$  is the average refractive index,  $n_1$  is the modulation parameter,  $K$  is the modulus of the grating vector defined as  $2\pi/\Lambda$ , with  $\Lambda$  being the grating period and  $\varphi$  the angle of the fringe planes. The grating vector makes an angle of  $0^\circ$  with the  $y$  axis for non-slanted reflection gratings as can be seen in Fig. 1a, whereas for pure transmission gratings the grating vector makes an angle of  $90^\circ$  with the  $y$  axis (Fig 1b).

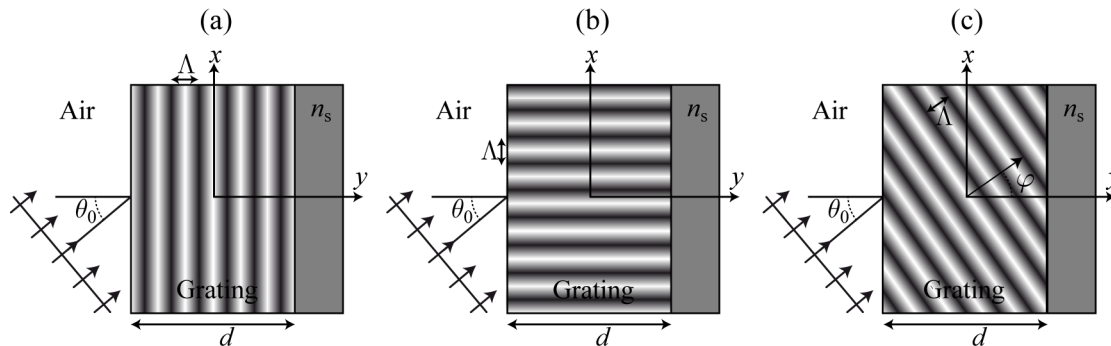


Figure 1. (a) Pure reflection volume diffraction grating scheme. (b) Pure transmission volume diffraction grating scheme. (c) Slanted volume diffraction grating scheme.

These devices have a great number of applications such as data storage<sup>7</sup> and fiber optics coupling<sup>12</sup>.

Concerning TFFs, a set of High-Reflection Coatings (HRCs) have been analyzed with both FDTD and the Characteristic Matrix Method (CMM). HRC is a basic type of TFF and is composed by a stack of alternate high- and low-index dielectric films, all one quarter wavelength thick as it has been illustrated in Fig. 2.

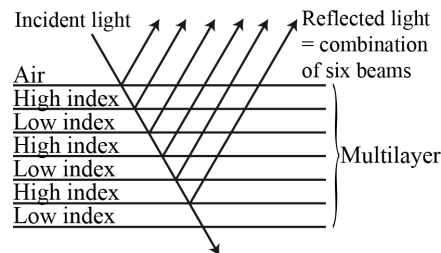


Figure 2. High-reflectance coating scheme[2].

Light reflected within the high-index layers do not suffer any phase shift while a change of  $180^\circ$  in the low-index layers is produced. It is straightforward to see that the light produced by reflection at successive boundaries throughout the assembly reappears at the front surface all in phase so that they recombine constructively. To ensure this behavior the optical thickness of the film should be made one quarter wavelength. The optical thickness of a thin film is directly related with the refractive index, the wavelength and the angle of incidence. HRCs have many applications such as photovoltaic cells<sup>9</sup> and Microelectromechanical Systems<sup>10</sup>.

The good agreement between the results obtained from the FDTD method and the Characteristic Matrix Method (CMM) validates the numerical implementation and gives the possibility of simulating a wide spectrum of optical devices based on dielectric structures.

In the Section 2 we will give a brief review of the theory used in this work. In Section 3 the results obtained from the analysis of VHG and TFF by means of the FDTD and their comparison with exact curves is given. Finally, in Section 4 the conclusions derived from the results are summarized.

## 2. THEORY

A brief review of the Finite-Difference Time-Domain method and the CMM is given. The strategies followed for reducing the time costs of the FDTD method are also detailed. These strategies are based on the use of the Single Instruction Multiple Data (SIMD) registers available in modern microprocessors and the shared memory approach defined by OpenMP directives.

### 2.1 Finite-Difference Time-Domain method

Light propagation is described by means of Maxwell's time-dependent curl equations:

$$\begin{aligned}\frac{\partial \tilde{\mathbf{D}}}{\partial t} &= \frac{1}{\sqrt{\epsilon_0 \mu_0}} \nabla \times \mathbf{H}, \\ \tilde{\mathbf{D}}(\omega) &= \epsilon_r(\omega) \tilde{\mathbf{E}}(\omega), \\ \frac{\partial \mathbf{H}}{\partial t} &= -\frac{1}{\sqrt{\epsilon_0 \mu_0}} \nabla \times \tilde{\mathbf{E}},\end{aligned}\quad (2)$$

where  $\epsilon_0$  is the electrical permittivity in farads per meter,  $\epsilon_r$  is the medium relative complex permittivity constant, that has been assumed real,  $\mu_0$  is the magnetic permeability in henrys per meter. The flux density is denoted by  $\tilde{\mathbf{D}}$  and both,  $\tilde{\mathbf{D}}$  and  $\tilde{\mathbf{E}}$  are normalized with respects to the vacuum impedance:

$$\eta_0 = (\mu_0 / \epsilon_0)^{1/2}. \quad (3)$$

The FDTD algorithm used here is based on the Yee<sup>13</sup> lattice. The electrical field components  $\mathbf{E}$  and the magnetical field components  $\mathbf{H}$  are centered in a bidimensional cell so that every  $\mathbf{E}$  component is surrounded by four circulating  $\mathbf{H}$  components, and every  $\mathbf{H}$  component is surrounded by four circulating  $\mathbf{E}$  components [12-14].

As a result, the Maxwell's curl equations can be discretized and solved by using the central-difference expressions, for both the time and space derivatives. So, the Eq. (2) can be reformulated as follows:

$$\tilde{D}_z|_{i,j}^{n+1/2} = \tilde{D}_z|_{i,j}^{n-1/2} + \frac{\Delta t}{\sqrt{\epsilon_0 \mu_0}} \left( \frac{H_y|_{i+1/2,j}^n - H_y|_{i-1/2,j}^n}{\Delta x} - \frac{H_x|_{i,j-1/2}^n - H_x|_{i,j+1/2}^n}{\Delta y} \right), \quad (4)$$

where  $\Delta x$  and  $\Delta y$  are the spatial and time resolution respectively.

In order to simulate unbounded free space, it must be included a formalism in order to avoid the interferences produced by outgoing waves reaching the grid simulation limits. For this reason a simplified version of the Perfectly Matched Layers (PML) developed by Berenger<sup>14,15</sup> has been implemented in this work<sup>16,17</sup>. The PMLs are a good technique for the absorption of electromagnetic waves by means of a nonphysical absorbing medium adjacent to the outer FDTD mesh boundary. The basic idea of this formalism is to create a medium that is lossy and minimize the amount of reflection between vacuum and the PML region.

Related with the illumination method, note that the incidence is assumed to be from air to medium. In connection with the propagation in the FDTD region, it must be said that the source is introduced along the connecting boundary by using a Total Field/Scattered Field (TF/SF) algorithm<sup>18-20</sup>, where the linearity of Maxwell's equations and their decomposition of the electromagnetic field are assumed:  $(\mathbf{E}; \mathbf{H})_{\text{Total}} = (\mathbf{E}; \mathbf{H})_{\text{inc}} + (\mathbf{E}; \mathbf{H})_{\text{scat}}$ . Where  $(\mathbf{E}; \mathbf{H})_{\text{inc}}$  are the values of the incident field, which are assumed to be known at all space points in the FDTD grid and also at all time steps.  $(\mathbf{E}; \mathbf{H})_{\text{scat}}$  are the values of the scattered wave fields, which are unknown and produced by the optical device in our particular case. A simple approach to calculate the incident field values for arbitrary wave angles of incidence is based upon a look-up table procedure<sup>18</sup>. This method avoids the computation of the incident wave in the whole bidimensional grid and only two one-dimensional arrays are needed. In Fig. 3 the electric field  $E_z$  for a specific time step of a HVG simulation is shown. Also the diffraction grating, the TF/SF area and the PML region can be easily identified.

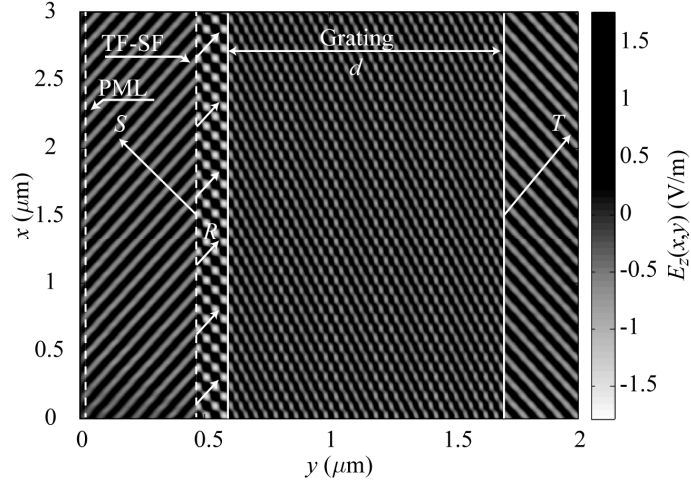


Figure 3. Electric field  $E_z$  of a reflection diffraction grating simulation. Parameters:  $d=11.08 \mu\text{m}$ ,  $\Lambda=0.22 \mu\text{m}$ ,  $n_0=1.63$ ,  $n_1 = 0.025$ ,  $n_s=1$ ,  $\theta_0=32.4^\circ$ ,  $\lambda=633 \text{ nm}$ ,  $\Delta=0.32 \text{ m}$ ,  $\Delta t = 4.74 \cdot 10^{-6} \text{ ns}$ .

Although, note that in this work, the truncation of the TF/SF is done in order to reduce the artifacts produced by the superposition of the grating and the connecting conditions. A similar approach is detailed in<sup>19,20</sup>. This truncation needed because of evaluating the connecting conditions in the interface overlapped with the grating produce a set of undesired artifacts travelling a long the grating. Therefore, the Total Field region is limited to the input plane of the grating and the incident plane wave is not suppressed at the output plane of the grating.

## 2.2 Paralelization and vectorization of the FDTD method

The use of The Single Instruction Multiple Data (SIMD) instructions in general purpose processors was promoted by Intel in 1999 due to the increasing PC volume market. This is the most cost-effective way of accelerating floating-point performance in general purpose processors, and it permits a theoretical full x4 performance gain (full 4-wide SIMD operation can also be done every clock cycle) for single precision data, although 2x is the typical gain on real applications due to other factors such as memory access and other tasks<sup>8</sup>. In order to be effective during the computation, the pointers in memory of the array to be used by SIMD instructions must be aligned. For that reason, the allocation of the memory for a matrix with  $r$  rows and  $m$  columns has been done in a single aligned column vector. The matrix that stores the displacement vector in  $z$  direction can be defined as follows:

$$\tilde{\mathbf{D}}_z^{n+1/2} = D_z \Big|_{i,j}^{n+1/2} = \left[ \tilde{\mathbf{d}}_z^0 \quad \tilde{\mathbf{d}}_z^1 \quad \dots \quad \tilde{\mathbf{d}}_z^{m-1} \right]^{n+1/2}, \quad (5)$$

where  $\mathbf{d}_z^j = [d_z[0] \quad d_z[1] \quad \dots \quad d_z[r-1]]^T$  with  $T$  denoting the hermitian transpose matrix. On the other hand, the time is going to be suppressed from the formulation due to the fact that in the software only one matrix related with the values of each component field is stored. The next values are computed from the previous values stored in the same matrix and it is not necessary to store the previous values in auxiliary structures.

This vectorial scheme permits to exploit the SSE registers in the CPU and also to improve the performance of the method. The Eq. (4) can be redefined taking into account the storage scheme detailed before and the Eq. (5):

$$d_z^j[i] = d_z^j[i] + c_d[i] \left( h_y^j[i] - h_y^j[i-1] - h_x^j[i] + h_x^{j-1}[i] \right), \quad (6)$$

where  $i = 0, 1, \dots, r-1$  and is evaluated in blocks of four and  $j = 1, 2, \dots, m-1$ . The coefficient array  $\mathbf{C}_d$  contain values related with also spatial-time resolution and physical media as can be easily identified in Eq. (4). Note that the classical implementation of the Eq. (4) requires a pair of loops for updating the field component in each cell. With this rearrangement, it is suppressed one loop and the field is computed in groups of four in the same time that one cell is solved in the sequential implementation.

Furthermore, the Eq. (6) can be evaluated in parallel due to the fact that this equation only modifies the values of the displacement vector. Therefore, a shared memory approach based on OpenMP<sup>21</sup> has been used in order to parallelize the main loops of the method. This parallelization is possible due to the fact that the FDTD method solves  $\mathbf{D}_z$  field using the inner  $\mathbf{D}_z$ , the  $\mathbf{H}_x$  and  $\mathbf{H}_y$  data previously stored in the computer memory. Applying OpenMP directives, the loop that is in charge of computing each field can be completed by several threads distributing the total number of iterations between the cores available in the microprocessor. These threads are free of dependences. Therefore, each field update can be parallelized since the dependent parameters are shared in memory.

### 2.3 Characteristic Matrix Method

The Fig. 4 illustrates the arrangement, in which the CMM method is based on. The CMM links the tangential components of  $\mathbf{E}$  and  $\mathbf{H}$  at the incident surface with the tangential components of  $\mathbf{E}$  and  $\mathbf{H}$  which are transmitted through this interface. This is accomplished by means of a 2x2 matrix denoted as the characteristic matrix of the thin film.

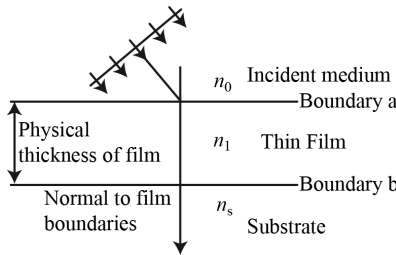


Figure 4. Plane wave incident on a thin film<sup>2</sup>.

$$\begin{bmatrix} E_a \\ H_a \end{bmatrix} = \begin{bmatrix} \cos \delta & (i\eta_1 \sin \delta) / \eta_1 \\ i\eta_1 \cos \delta & \cos \delta \end{bmatrix} \begin{bmatrix} E_b \\ H_b \end{bmatrix}, \quad (7)$$

with  $\eta_1$  as the optical admittance defined as the difference between  $H$  and  $E$ ,  $\delta$  is the phase of the layer and is defined as follows:

$$\delta = 2\pi n_1 d \cos \theta_1 / \lambda, \quad (8)$$

with  $d$  and  $n_1$  being the physical thickness and the refractive index of the film respectively and also detailed in Fig. 4. If  $\theta_0$  is the angle of incidence, the value of  $\theta_1$  can be calculated from Snell's Law,

$$n_0 \sin \theta_0 = n_1 \sin \theta_1 = n_s \sin \theta_s. \quad (9)$$

This result can be immediately extended to the general case of an assembly of  $q$  layers, when the characteristic matrix is simply the product of the individual matrices taken in correct order, i.e.

$$\begin{bmatrix} B \\ C \end{bmatrix} = \left\{ \prod_{r=1}^q \begin{bmatrix} \cos \delta_r & (i\eta_r \sin \delta_r) / \eta_r \\ i\eta_r \cos \delta_r & \cos \delta_r \end{bmatrix} \right\} \begin{bmatrix} 1 \\ \eta_s \end{bmatrix}, \quad (10)$$

where  $\delta_r = 2\pi n_r d_r \cos \theta_r / \lambda$ ,  $\eta_r = (\epsilon_0 / \mu_0)^{1/2} n_r \cos \theta_r$  for TE polarization. Note that also a normalization of the Eq. (8) has been done dividing through  $E_b$ . So that  $B = E_d / E_b$  and  $C = H_d / E_b$ .

Let  $Y$  be  $C/B$ , and the reflectance of the optical component is

$$R = \left( \frac{\eta_0 - Y}{\eta_0 + Y} \right) \left( \frac{\eta_0 - Y}{\eta_0 + Y} \right)^*. \quad (11)$$

Therefore, the application of Eq. (10) to a stack of thin dielectric layers is straightforward. In the same manner, a VHG with a sinusoidal variation of its refractive index can be approximated by a large number of lamellar layers, and it can be regarded as a stack of homogeneous thin films.

## 2.4 Analysis of reflection gratings by means of the Mathieu matrix approach

One of the most popular theories to calculate the efficiency of the orders that propagate inside a diffraction grating is the Kogelnik's Coupled Wave Theory<sup>22</sup> and the Rigorous Coupled Wave Theory developed by Moharam and Gaylord<sup>23-26</sup>. The Kogelnik's CWT provides analytical expressions for the zero and first order for volume phase gratings and it is widely used by researchers because of it can provide exact predictions under several conditions. The RCWT does not disregard second derivatives and also allows considers higher orders, therefore their results are more accurate and it can be applied to a wider range of applications. Nevertheless, the RCWT is not valid for non-slanted reflection gratings. In this case, the modulation is no longer infinitely periodic since it has only a finite number of cycles. That causes the grating not to be strictly periodic and the Floquet Theorem, which is the basis for the modal and the coupled-wave analysis, can not be applied.

Recently a matrix-method approach has been used to evaluate the electromagnetic wave transmission for reflection gratings with arbitrary angle of incidence<sup>27</sup>. Basically, the idea is to define a matrix which characterize the medium, linking the electromagnetic field components and their derivatives at an interface between two adjoining layers.

The periodic medium extends from  $y = y_1$  to  $y = y_2$ , and the electric field inside it verifies the following second order differential equation:

$$\frac{d^2 E}{dy^2} + (k_0^2 n(y)^2 - k_x^2) E = 0. \quad (12)$$

This equation can be solved by means of two linearly independent solutions  $E_{c1}$  and  $E_{c2}$ ,

$$\begin{pmatrix} E(y_2) \\ \frac{dE(y_2)}{dy} \end{pmatrix} = \mathbf{M} \begin{pmatrix} E(y_1) \\ \frac{dE(y_1)}{dy} \end{pmatrix} = \begin{pmatrix} m_{11} & m_{12} \\ m_{21} & m_{22} \end{pmatrix} \begin{pmatrix} E(y_1) \\ \frac{dE(y_1)}{dy} \end{pmatrix}, \quad (13)$$

where the layer matrix  $\mathbf{M}$  can be built linking the fields and their derivatives at two different values of  $y$  as is detailed in Lekner's discussion<sup>28</sup>.

On the other hand, one should notice that the Eq. (12) can be transformed into the Mathieu equation:

$$\frac{d^2 E}{du^2} + [a - 2q \cos(2u)] E = 0, \quad (14)$$

provided the following change of variables:

$$\begin{aligned} u &= \frac{Ky}{2}, \\ a &= \frac{4}{K^2} (k_0^2 n_0^2 - k_x^2), \\ q &= -\frac{2}{K} k_0^2 n_1^2, \end{aligned} \quad (15)$$

Two linearly independent solutions of Eq. (14) are the Mathieu cosine  $C_m(a, q, u)$  and the Mathieu sine  $S_m(a, q, u)$ . Therefore, any solution of (12) can be put in the form:

$$E(y) = AC_m(a, q, u) + BS_m(a, q, u) \quad (16)$$

Applying the boundary conditions of the electric field for the specific case of a volume reflection grating of thickness  $d$  ( $y_1 = 0$  and  $y_2 = d$ ), the reflection and transmission amplitudes can be obtained as:

$$R = \frac{k_y^l k_y^H m_{12} + m_{21} + j k_y^l m_{22} - j k_y^H m_{11}}{k_y^l k_y^H m_{12} - m_{21} + j k_y^l m_{22} - j k_y^H m_{11}},$$

$$T = e^{-jk_y^H d} \frac{2 j k_y^l}{k_y^l k_y^H m_{12} - m_{21} + j k_y^l m_{22} - j k_y^H m_{11}},$$
(17)

Where the efficiency of the reflected order  $DE_{-1}$  can be obtained as  $|R|^2$  and the efficiency of the transmitted one as the real part of  $(k_z^H / k_z^l) |T|^2$ .

### 3. RESULTS AND DISCUSSION

In this section the results related with the computational optimization and the analysis of different diffractive optical elements are shown. First, the degree of improvement in terms of time simulation costs of the FDTD method is detailed. Second, different reflection holographic diffraction gratings are analyzed varying the substrate at the output plane of the gratings and also the spatial resolution of both numerical methods: FDTD and CMM. Third, transmission diffraction gratings are studied as a function of the angles of the reconstruction beam and the fringes planes. These cases are analyzed by means of two videos that show the behavior of the electromagnetic field as a function of these parameters. Finally, the reflectance of a set of High-reflection coatings is shown. The reflectance is computed by the FDTD method and it is compared with the analytical curves obtained with the CMM.

#### 3.1 Computational optimization results

Table 1 shows time simulation for the sequential and the optimized version of the FDTD implemented, also the SpeedUp is given, which is defined as the ratio between the sequential and parallel time costs. The computational results shown in Table 1 can be summarized in a SpeedUp that tends to four as the simulation size becomes greater. The grid in all cases has been defined as a square array of Yee cells.

It must be said that the sequential time costs of the FDTD method implemented is smaller compared with classical implementations of the method. Because of the fact that a correct usage of pointers and memory alignment was considered in the sequential version, modern compilers introduce successfully auto-vectorization rules that reduce the time costs of the sequential version in great manner. Therefore, the SpeedUp obtained can be considered greater (x2) if it is compared with classical implementation of the method. Although, in this work, the sequential version considered is the auto-vectorized version that it is considered as the maximum performance that can be obtained by a sequential implementation of the numerical method. These results are obtained by means of a CPU Intel i7-950 and 6 GB of DDR3-1333.

Table 1: Time simulation of the sequential version of the FDTD method compared with the parallel-vectorized version.

MCells	T <sub>seq</sub> (s)	T <sub>SSE+OpenMP</sub> (s)	SpeedUp
1.65	72.03	22.50	3.2
3.29	167.61	45.42	3.7
4.94	243.21	67.84	3.6
9.88	545.93	137.02	4
16.47	973.55	239.90	4.1

### 3.2 Reflection holographic gratings

Regarding VHG, here is presented the diffraction efficiency of the diffracted order of a reflection grating with the same scheme detailed in Fig. 1a. Fig. 5 shows the good agreement achieved between both numerical methods. Although, there exists slight difference between the two curves, produced by the finite transversal dimensions of the VHG when using the FDTD method compared with the infinite plane of incidence assumed in the CMM. Therefore, an analysis of the precision of the FDTD method has been performed.

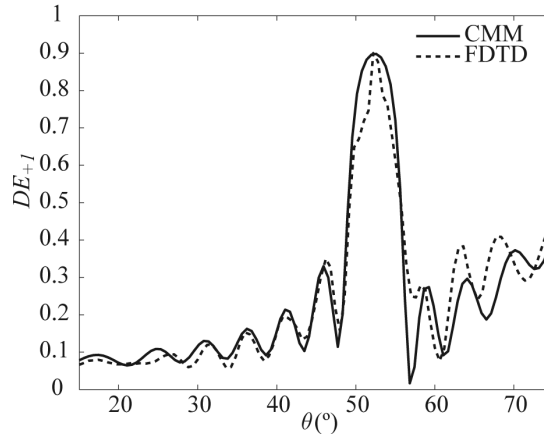


Figure 5. Comparison of the reflectance of a volume diffraction grating as a function of the angle of incidence. The output plane has been substituted by a transparent substrate with refractive index  $n_0$ . In both cases the parameters are:  $d=11.08 \mu\text{m}$ ,  $\Lambda=0.22 \mu\text{m}$ ,  $n_0=n_s=1.63$ ,  $n_1=0.025$ ,  $\lambda=633 \text{ nm}$ ,  $\Delta=0.32 \text{ nm}$ ,  $\Delta t=52.75 \cdot 10^{-9} \text{ ns}$ .

Both, the CMM and also the FDTD require a discretization of the medium by means of a dielectric homogeneous layer or the Yee cell, respectively. For that reason, an analysis of the same reflection diffraction grating with different samples per grating period is shown in Fig. 6. Specifically, Fig. 6 shows the diffraction efficiency of a grating surrounded by air. This implies that the output substrate shown in Fig. 1a is substituted by air. For this scheme, the CMM and FDTD methods are compared with the Coupled Wave Theory developed by Kogelnik<sup>22</sup> and also with a recent method based on the Mathieu functions<sup>27</sup>. Results obtained with the Mathieu functions can be considered as the reference results since they considered the continuous non-sampled set of fringes composing the VHG. It also considers an infinitely plane of incidence for the transversal dimension of the grating, such as Kogelnik's CWT and the CMM. Fig. 6a shows the diffraction efficiency obtained by the FDTD and the CMM methods with four samples per grating period, whereas in Fig. 6b the same curves are obtained with eight samples per period. As the number of samples is greater, the differences between the numerical and analytical curves far from the Bragg angles are reduced. Although, as can be seen in Fig. 6 all methods provide good results near from the Bragg angle. It is interesting to identify how the CW theory developed by Kogelnik is inefficient when modeling this specific set of reflection gratings.

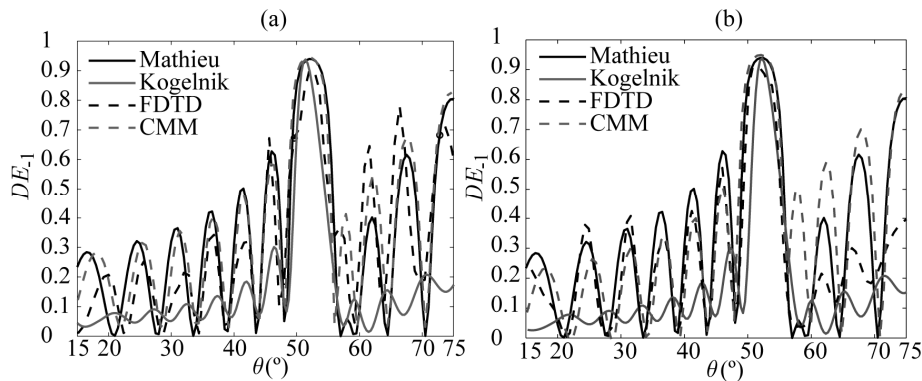


Figure 6. Angular selectivity. Parameters:  $d=11.08 \mu\text{m}$ ,  $\Lambda=0.22 \mu\text{m}$ ,  $n_0=1.63$ ,  $n_s=1$ ,  $n_1=0.025$ ,  $\lambda=633 \text{ nm}$ ,  $\Delta=0.32 \text{ m}$ ,  $\Delta t=52.75 \cdot 10^{-9} \text{ ns}$ . (a) 4 samples per grating period in FDTD and CMM. (b) 8 samples per grating period in FDTD and CMM.

### 3.3 Transmission holographic gratings

For showing the performance of the method for slanted gratings it has been performed an animation based on a set of simulations varying the angle of the fringe planes (Fig. 1c). This sequence permits to identify how the diffracted order becomes greater when the angle of the interference pattern is 90° degrees (pure transmission grating scheme illustrated in Fig. 1b). In order to analyze superior orders, the interference pattern inside the grating has been modified respect to the Eq. (1). Taking into account the relation between the refractive index parameter and the relative electrical permittivity of a medium ( $n=\epsilon_r^{1/2}$ ):

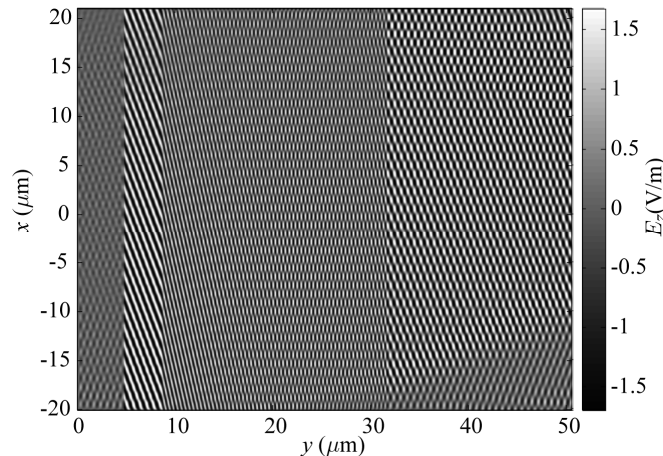
$$\epsilon(x, y) = \epsilon_0 + \epsilon_1 \cos[K(\cos \phi y + \sin \phi x)] + \epsilon_2 \cos[K(\cos \phi y - \sin \phi x)], \quad (11)$$

where  $\epsilon_1$  and  $\epsilon_2$  are the modulation parameters. The physical parameters of the transmission VHG analyzed in this section have been summarized in Table 2.

Table 2: Physical parameters of the transmission grating analyzed and set up of the FDTD method.

Grating				FDTD			
$\Lambda$	$\epsilon_1$	$\epsilon_2$	$d$	$\lambda$	$\Delta$	$\Delta t$	MCells
0.89 $\mu\text{m}$	0.0395	0.0064	23 $\mu\text{m}$	633 nm	15.83 nm	26.38·10 <sup>-9</sup> ns	12.52

The  $E_z$  field component as a function of the slanting angle is detailed in the sequence shown in Video 1.

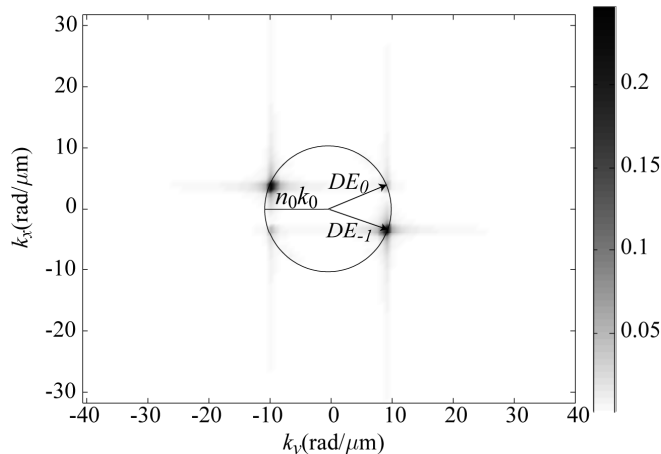


Video 1. Animation of a sequence obtained from a simulation of a transmission VHG varying the angle of the fringe planes.

It can be identified a maximum of the diffraction order near 90° degrees (pure transmission diffraction grating):

<http://dx.doi.org/10.1117/12.896873.2>

Moreover, the output of the transmission diffraction grating has been analyzed as a function of the angle of incidence of the reconstruction beam ( $\theta_0$ ). The  $k$ -space permits to easily identify the different plane waves present in a specific region. Varying the angle of incidence, the different orders and their position is modified also in amplitude and in position a long the circle of radius  $n_0 k_0$ . This circle is known as the Ewald's circle and it is directly related with the Floquet's expansion inside the periodic media.



Video 2. Animation of a sequence obtained from a simulation of a pure transmission VHG ( $\varphi=90^\circ$ ) varying the angle of incidence  $\theta$ . The  $k$ -space is represented and it can be identified a maximum of the first diffracted order near  $\theta=21^\circ$  and a maximum of the second diffracted order near of  $\theta=45^\circ$ : <http://dx.doi.org/10.1117/12.896873.1>

The comparison between numerical and experimental values is shown in Fig. 7. The first diffracted order and the second diffracted order obtained by means of the FDTD method and measurements are represented. As can be seen a good approach between numerical and experimental values is achieved, thus validating our implementation.

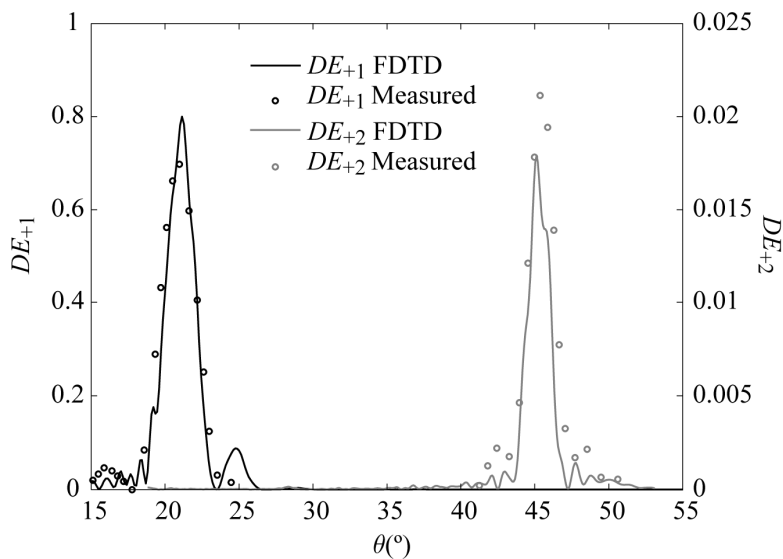


Figure 7. Angular selectivity. Parameters:  $d=11.08 \mu\text{m}$ ,  $\Lambda=0.22 \mu\text{m}$ ,  $n_0=1.63$ ,  $\lambda=633 \text{ nm}$ ,  $\Delta=0.32 \text{ m}$ ,  $\Delta t = 4.74 \cdot 10^{-6} \text{ ns}$ . (a) 4 samples per grating period in FDTD and CMM. (b) 8 samples per grating period in FDTD and CMM.

### 3.4 High-reflecting coating analysis

On the other hand, Fig. 8 shows reflectance of four different HRCs as a function of the normalized wavelength. More specifically, it has been simulated a set of stacks that alternate  $\lambda_0/4$  layers of high- and low-index. Note that in each graph an illustration of each stack is detailed, in which by means of a gray scale is illustrated the different layers and their position in the HRC. In all cases, the device ends with a transparent substrate.

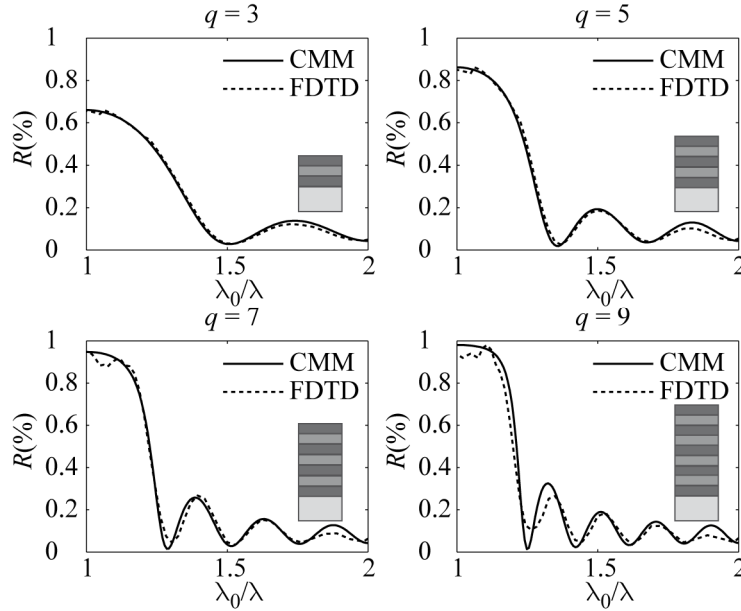


Fig. 8: Reflectance  $R$  for normal incidence of alternating  $\lambda_0/4$  layers of high- ( $n_H = 2.3$ ) and low-index ( $n_L = 1.38$ ) dielectric materials on a transparent substrate ( $n_s = 1.52$ ) as a function of the wavelength ratio  $\lambda_0/\lambda$ . FDTD Parameters:  $\lambda_0 = 460$  nm,  $\Delta = 2.3$  nm,  $\Delta t = 3.83 \cdot 10^{-9}$  ns.

#### 4. CONCLUSIONS

An improved version of the FDTD method based on SSE and OpenMP has been developed. This parallel-vectorial version achieves an improvement with respect to sequential version being till four times faster. In addition, the FDTD method has been successfully applied to simulating diffractive optical elements such as Volume Holographic Gratings and High-Reflectance Coatings. In both cases the FDTD method has been compared with a method based on the Characteristic Matrix of a layer. The VHG have been analyzed in reflection, transmission and also for slanted schemes. Specifically, for reflection gratings, the finite spatial resolution and its effect in the analysis of the reflectance as a function of the angle of incidence has been studied, identifying that for smaller spatial resolutions in both FDTD and CMM methods, the discrepancies between analytical curves becomes grater. Nevertheless, the numerical curves near the Bragg angle are quite close to theoretical curves. Furthermore, for this case of gratings, it has been demonstrated that modifying the output substrate can compromise the performance of classical formalisms such as the Coupled Wave theory developed by Kogelnik. The diffraction efficiency for transmission VHG has been also obtained by means of the FDTD method. In this case, it has been studied the influence of the slanting angle of the fringe planes and also the effect of the angle of incidence in the output plane. Therefore, a wider analysis of the  $k$ -space at the output plane has been performed obtaining the first and the second Bragg diffracted orders. These curves have been compared with experimental measurements of real gratings with similar characteristics, achieving good results. Finally, a set of High-Reflection coatings have been analyzed as a function of the wavelength by the FDTD method and the CMM. In all cases the numerical results are close to the theoretical values, thus demonstrating the potential of the numerical method and its capabilities on modeling a wide range of diffractive optical devices. The reduction of the time costs of the simulations also permits to simulate bigger areas and therefore to analyze more exhaustively the characteristics of this type of media and devices.

*Acknowledgements:* This work was supported by the "Ministerio de Ciencia e Innovación" of Spain under projects FIS2008-05856-C02-01 and FIS2008-05856-C02-02.

## REFERENCES

- [1] Fabry, C., and Perot A. N., "Théorie et applications d'une nouvelle méthode de spectroscopie interférentielle," *Ann. Chim. Phys* 16, 115-44 (1899)
- [2] Macleod, H. A., [Thin-Film Optical Filters], Institute of Physics Publishing., Bristol & Philadelphia, 5-188, (2002)
- [3] Brooks, R. E., Helflinger, L. O. and Werker, R. F., "9A9-Pulsed laser holograms," *IEEE J. Quatn. Electron*, 2(8), 275-279 (1966).
- [4] Burch, J. M. and Palmer, D. A., "Interferometric methods for the photographic production of large gratings," *Journal of Modern Optics* 8(1), 73-80 (1961).
- [5] Collier, R. J. and Pennington, K. S., "Multicolour imaging from holograms formed on two-dimensional media," *Appl. Opt.* 6(6), 1091-1095 (1967).
- [6] Kaverhrad, M. and Jivkova, S., "Indoor broadband optical wireless communications: optical subsystems designs and their impact on channel characteristics," *Wireless Communications* 10(2), 30-35 (2003).
- [7] Ashley, J., Bernal, M.-P., Burr, G. W., Coufal, H., Guenther, J. A., Hoffnagle, J. A., Jefferson, C. M., Marcus, B., Macfarlane, R. M., Shelby, R. M. and Sincerbox, G. T., "Holographic data storage technology," *IBM Journal of Research and Development* 44(3), 341-368 (2000).
- [8] Shreekant, T. and Huff, T., "The Internet Streaming SIMD Extensions," *Intel Tecnology Journal* Q2, 1-8 (1999).
- [9] Esteban, R., Laroche, M. and Greffet, J. J., "Dielectric gratings for wide-angle, broadband absorption by thin film photovoltaic cells," *Applied Physics Letters* 97(22), 221111 - 221111-3 (2010).
- [10] Helmbrecht, M. A., "Optical coatings for MEMS devices," *Proc. of Lasers and Electro-Optics and Quantum Electronics and Laser Science Conference*, 1-2 (2010).
- [11] Solymar, L. and Cooke, D. J., [Volume holography and volume gratings], Academic Press, London, 45-68 (1981).
- [12] Tibuleac, S., Wawro, D. and Magnuson, R., "Resonant diffractive structures integrating waveguide-gratings on optical fiber endfaces," *Proc. LEOS* 2, 874 (1999).
- [13] Yee, K. S., "Numerical solution of initial boundary value problems involving Maxwell's equations in isotropic media," *IEEE Trans. On Antennas and Propagation* 14(3), 303-307 (1996).
- [14] Berenger, J. P., "A perfectly matched layer for the absorption of electromagnetic waves," *J. Comput. Phys.*, 114(2), 185-204 (1994).
- [15] Berenger, J. P., "Three-dimensional perfectly matched layer for the absorption of electromagnetic waves," *J. Comput Phys.*, 127(2), 363-379 (1996).
- [16] Sullivan, D. M., [Electromagnetic simulation using the FDTD method], IEEE Press Editorial Board, (2000).
- [17] Sullivan, D. M., "A simplified PML for use with the FDTD method," *IEEE Microwave and Guided Wave letters* 6(2), 97-99 (1996).
- [18] Taflove, A., [Computational electrodynamics: The Finite-Difference Time-Domain Method], Artech House Publishers, (1995).
- [19] Francés, J., Pérez-Molina, M., Neipp, C. and Beléndez, A., "Rigorous interference and diffraction analysis of diffractive optic elements," *Comput. Phys. Commun.* 182(12), 1963-1973 (2010).
- [20] Jiang, Y.-N., Ge D-B. and Ding, S. J., "Analysis of TF-SF boundary for 2D-FDTD with plane p-wave propagation in layered dispersive and lossy media," *Progr. Electromagn. Res.* 83(12), 157-172 (2008).
- [21] Yan, J., He, J., Han, W. and Chen, W., "How OpenMP Applications Get More Benefit from Many-Core Era," *Proc. of International Workshop on OpenMP 2010*, 6132, 83-95 (2010).
- [22] Kogelnik, H., "Coupled Wave Theory for thick hologram gratings," *Bell Syst. Tech. J.* 48(9), 2902-2947 (1969).
- [23] Moharam, M. G. and Gaylord, T. K., "Rigorous coupled-wave analysis of planar-grating diffraction," *J. Opt. Soc. Am.* 71(7), 811-818 (1981).
- [24] Moharam, M. G. and Gaylord, T. K., "Rigorous coupled-wave analysis of grating diffraction-e-mode polarization and losses," *J. Opt. Soc. Am.* 73(4), 451-455 (1983).
- [25] Moharam, M. G. and T. K. Gaylord, "Three-dimensional vector coupled-wave analysis of planar-grating diffraction," *J. Opt. Soc. Am.* 73(9), 1105-1112 (1983).
- [26] Moharam, M. G. and T. K. Gaylord, "Analysis and applications of optical diffraction by gratings," *Proc. IEEE* 73(5), 894-937 (1985).

- [27] Francés, J., Neipp, C., Márquez, A., Beléndez, A. and Pascual, I., "Analysis of reflection gratings by means of a matrix method approach," *Prog. Electromagn. Res.* 118, 168-183 (2011).
- [28] Lekner, J., [Theory of Reflection of Electromagnetic and Particle Waves], Kluwer Academic Publishers Group, (1987).